Journal of
Applied Remote Sensing

RemoteSensing.SPIEDigitalLibrary.org

Azimuth-range decouple-based L_1 regularization method for wide ScanSAR imaging via extended chirp scaling

Hui Bi
Bingchen Zhang
XiaoXiang Zhu
Wen Hong

SPIE.

Hui Bi, Bingchen Zhang, XiaoXiang Zhu, Wen Hong, "Azimuth-range decouple-based L_1 regularization method for wide ScanSAR imaging via extended chirp scaling," *J. Appl. Remote Sens.* **11**(1), 015007 (2017), doi: 10.1117/1.JRS.11.015007.

Azimuth-range decouple-based L_1 regularization method for wide ScanSAR imaging via extended chirp scaling

Hui Bi,[a,b,*] Bingchen Zhang,[a] XiaoXiang Zhu,[c,d] and Wen Hong[a]

[a]Institute of Electronics, Science and Technology on Microwave Imaging Laboratory, Chinese Academy of Sciences, No. 19, North 4th Ring Road West, Haidian District, Beijing 100190, China

[b]University of Chinese Academy of Sciences, No. 19, Yu Quan Road, Beijing 100049, China

[c]Remote Sensing Technology Institute, German Aerospace Center (DLR), Munchener Straße 20, Wessling 82234, Germany

[d]Technical University of Munich, Signal Processing in Earth Observation, Arcisstraße 21, Munich 80333, Germany

Abstract. In this paper, we proposed an azimuth-range decouple-based L_1 regularization method for wide ScanSAR imaging via extended chirp scaling (ECS) and applied it to the TerraSAR-X data to achieve large-scale sparse reconstruction. Compared with ECS, the conventional ScanSAR imaging algorithm based on matched filtering, the proposed method can improve the synthetic aperture radar image performance with full-sampling raw data for not only sparse but also nonsparse surveillance regions. It can also achieve high-resolution imaging for sparse considered scenes efficiently using down-sampling raw data. Compared with a typical L_1 regularization imaging approach, which requires transfer of the two-dimensional (2-D) echo data into a vector and reconstruction of the scene via 2-D matrix operation, our proposed method has less computational cost and hence makes the large-scale regularization reconstruction of considered area become possible. The experimental results via real data validate the effectiveness of the proposed method. [DOI: 10.1117/1.JRS.11.015007]

Keywords: synthetic aperture radar; wide ScanSAR; extended chirp scaling; compressive sensing; regularization; azimuth-range decouple.

Paper 16577 received Jul. 31, 2016; accepted for publication Dec. 27, 2016; published online Jan. 24, 2017.

1 Introduction

Synthetic aperture radar (SAR), an active microwave radar, when installed in a platform, e.g., an airplane or a satellite, transmits and receives electromagnetic waves producing high-resolution images of surveillance regions by the matched filtering (MF) method.[1,2] In modern SAR processing, wide-swath imaging is commonly used in marine monitoring, ship detection, etc. ScanSAR[3] provides a typical wide-swath SAR imaging mode, which increases the swath width by periodically switching the incidence angle of the antenna among different subswaths from near to far range. The data coverage of each subswath in one scanning period is called burst, i.e., the data in each subswatch consisting of a set of bursts obtained in all periods. The antenna will scan along the range several times, which will decrease the azimuth resolution. In other words, ScanSAR mode increases the swath by sacrificing the azimuth resolution. To further increase the swath width, TerraSAR-X introduces the new wide ScanSAR mode to achieve a broader range coverage of over 200 km.[4] Compared with ScanSAR, wide ScanSAR increases only the number of subswaths. The imaging geometry, formation, and reconstructed algorithm of it are identical to ScanSAR.

*Address all correspondence to: Hui Bi, E-mail: bihui1991@163.com

1931-3195/2017/$25.00 © 2017 SPIE

MF is the conventional SAR imaging method that needs to satisfy the Shannon–Nyquist sampling theory.[5,6] The Range–Doppler algorithm (RDA)[7] and the chirp scaling algorithm[8] are the well-known MF-based SAR-focusing approaches and have been widely used in the processing of SAR raw data. For ScanSAR, Moreira et al. developed an extended chirp scaling (ECS) algorithm in 1996,[9] which can achieve high-resolution imaging successfully. Compressive sensing (CS), an important development in sparse signal processing, proposed by Donoho et al.[10,11] is a technique that can recover the original signal even from far fewer samples than sampling theory required. Recently, sparse signal processing has been successfully applied in SAR imaging and obtained encouraging results in reconstructing high-resolution images via the L_1 regularization method. However, due to the range and azimuth are coupled in the SAR raw data, conventional L_1 regularization method requires much higher computational cost and therefore becomes impractical in wide-swath imaging. To solve the aforementioned problem, Zhang et al. introduced an azimuth-range decoupling method that can reduce the computational complexity of CS-based SAR imaging using a constructed approximated observation operator,[12] an inverse of the MF procedure, to replace the exact observation function, i.e., measurement matrix in CS, and then exploit $L_q(0 < q \leq 1)$ regularization technique to reconstruct the considered scene efficiently. In 2014, Fang et al. further demonstrated the above azimuth-range decoupling idea in detail using RDA as the example and applied it to Stripmap SAR imaging successfully.[13] The CS-SAR imaging[13] not only can acquire high-resolution images with down-sampling data but also can reduce the computational cost of the same order as the traditional MF-based SAR imaging methods.

Motivated by the above idea, in this paper, we proposed an ECS-based azimuth-range decouple L_1 regularization wide ScanSAR imaging approach. In this method, we exploit the echo simulation operator constructed based on the inverse procedure of the ECS algorithm to replace the exact observation matrix (measurement matrix) in the conventional L_1 regularization-based imaging procedure and then utilize the iterative thresholding algorithm (ITA)[14] to achieve iterative recovery of the considered scene.

The main contributions of the present work are as follows:

1. Exploiting full-sampling ScanSAR raw data, not only for sparse but also for nonsparse surveillance regions, our proposed method can improve SAR imaging performance efficiently compared with MF-based imaging approaches (e.g., ECS in this paper), e.g., sidelobe, noise, and clutter suppression, and has potential in super-resolving imaging.
2. Exploiting down-sampling ScanSAR raw data, for sparse surveillance regions, our proposed method can achieve high-resolution imaging from raw data domain, while MF-based approaches could not successfully reconstruct the considered scene using fewer measurements than the requirement of sampling theory. Compared with the conventional L_1 regularization imaging approach, our proposed method has less computational complexity and memory occupation and allows large-scale reconstruction of sparse considered area.
3. The proposed method is very helpful in practical ScanSAR system design. For large-scale sparse scene observation, e.g., ocean analysis, we can increase the swath width by decreasing pulse repetition frequency (PRF) appropriately, called azimuth down-sampling. The decrease of PRF will also reduce the system complexity efficiently. For the collected huge ScanSAR raw data with less PRF, our proposed method also can achieve reconstruction successfully.

The rest of this paper is organized as follows. Section 2 presents the wide ScanSAR imaging model and conventional L_1 regularization-based wide ScanSAR reconstruction method. Section 3 describes the proposed ECS-based azimuth-range decouple L_1 regularization mechanism for the wide ScanSAR imaging along with an iterative recovery algorithm and the analysis of the computational cost. Section 4 shows the experimental results via TerraSAR-X wide ScanSAR date. Conclusions are drawn in Sec. 5.

2 Wide ScanSAR Imaging Based on L_1 Regularization

As shown in Fig. 1, similar to ScanSAR, discarding the weighting coefficient that is the constant term, for one beam, the echo data $s(\eta, \tau)$ at time (η, τ) of wide ScanSAR can be expressed as

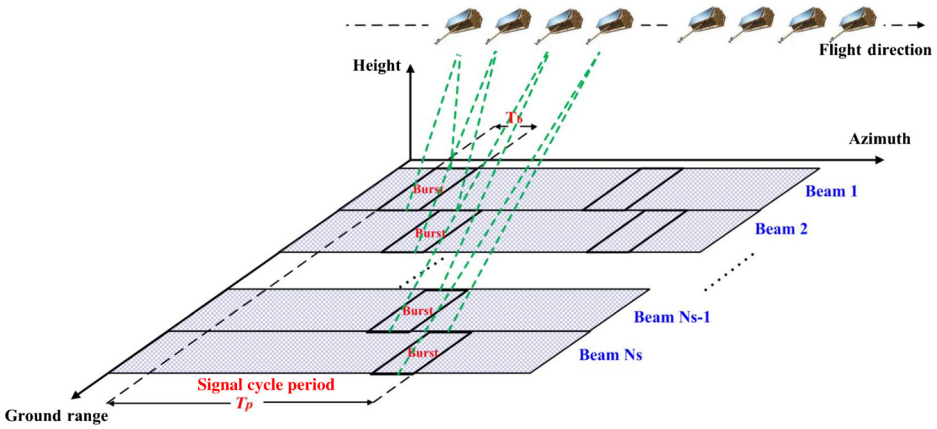

Fig. 1 Wide ScanSAR imaging geometry.

$$s(\eta,\tau)=\iint \sigma(p,q)\cdot\sum_{n}\mathrm{rect}\left(\frac{\eta-nT_p}{T_b}\right)\cdot\mathrm{rect}\left[\frac{\tau-2R(p,q,\eta)/c}{T_r}\right]$$

$$\cdot\exp\left[-j\pi\frac{4R(p,q,\eta)}{\lambda}\right]\cdot\omega\left[\tau-\frac{2R(p,q,\eta)}{c}\right]\mathrm{d}p\mathrm{d}q, \tag{1}$$

where η is the azimuth time, τ is the range time, and $\sigma(p,q)$ is the backscattered coefficient at point (p,q) in the considered scene with $1\le p\le N_P$, $1\le q\le N_Q$. c and λ are the speed of light and the wavelength, respectively. T_r is the transmitted pulse duration, T_b is the burst duration, T_p is the signal cycle period (or called synthetic aperture time), n is the burst index, $\omega(\tau)$ is transmitted signal, and $R(p,q,\eta)$ is the slant range. In this paper, we will perform the regularization-based wide ScanSAR imaging for each burst in turn and then combine the results of all bursts together to achieve a final image of the considered area. According to Eq. (1), the echo signal $y(\eta,\tau)$ in the specific burst can be represented as

$$y(\eta,\tau)=\iint \sigma(p,q)\cdot\mathrm{rect}\left(\frac{\eta}{T_b}\right)\cdot\mathrm{rect}\left[\frac{\tau-2R(p,q,\eta)/c}{T_r}\right]$$
$$\cdot\exp\left[-j\pi\frac{4R(p,q,\eta)}{\lambda}\right]\cdot\omega\left[\tau-\frac{2R(p,q,\eta)}{c}\right]\mathrm{d}p\mathrm{d}q. \tag{2}$$

We discreting the time series as $T_m(m=1,2,\ldots,M)$. Let $\mathbf{X}$ denotes an $N_P\times N_Q$ matrix whose (p,q) entry is $\sigma(p,q)$. Let $\mathbf{x}=\mathrm{vec}(\mathbf{X})$ with vectorization operation $\mathrm{vec}(\cdot)$ stacks the columns of $\mathbf{X}$. Let $[a]$ represents the floor of a nonnegative real number a. For $1\le n\le N$ with $N=N_P\times N_Q$, define $p_n=[(n-1)/N_P]+1$, $q_n=n-(p_n-1)N_P$. The nth entry of $\mathbf{x}$ is then $\sigma(p_n,q_n)$. Thus, we can obtain the discreting model as follows:

$$y(\eta_m,\tau_m)=\sum_{m=1}^{M}\sum_{n=1}^{N}\phi(m,n)\sigma(p_n,q_n), \tag{3}$$

with the wide ScanSAR measurement matrix $\mathbf{\Phi}=[\phi(m,n)]_{M\times N}$ of one burst being

$$\phi(m,n)\cong\iint_{(\eta,\tau)\in T_m}\mathrm{rect}\left(\frac{\eta}{T_b}\right)\cdot\mathrm{rect}\left[\frac{\tau-2R(p,q,\eta)/c}{T_r}\right]$$
$$\cdot\exp\left[-j\pi\frac{4R(p,q,\eta)}{\lambda}\right]\cdot\omega\left[\tau-\frac{2R(p,q,\eta)}{c}\right]h_m(\eta,\tau)\mathrm{d}\eta\mathrm{d}\tau, \tag{4}$$

where matrix $\mathbf{H}\cong\{h_m\}$ denotes the down-sampling operation, and the conventional wide ScanSAR radar observation matrix $\mathbf{\Theta}=[\theta(m,n)]_{M\times N}$ can be expressed as

$$\theta(m,n) = \text{rect}\left(\frac{\eta_m}{T_b}\right)\text{rect}\left[\frac{\tau_m - 2R(p_n,q_n,\eta_m)/c}{T_r}\right] \cdot \exp\left[-j\pi\frac{4R(p_n,q_n,\eta_m)}{\lambda}\right]\omega\left[\tau_m - \frac{2R(p_n,q_n,\eta_m)}{c}\right]. \tag{5}$$

Then, we can rewrite the wide ScanSAR imaging model as

$$\mathbf{y} = \mathbf{H}\boldsymbol{\Theta}\mathbf{x} + \mathbf{n}_0 = \boldsymbol{\Phi}\mathbf{x} + \mathbf{n}_0, \tag{6}$$

where $\mathbf{y} \in \mathbf{C}^{M\times 1}$ is the echo data, and $\mathbf{n}_0 \in \mathbf{C}^{M\times 1}$ is the thermal noise. If there is no down-sampling of echo data, $\mathbf{H}$ is an identity matrix.

In Eq. (6), if $\mathbf{x}$ is sparse enough and measurement matrix $\boldsymbol{\Phi}$ satisfies the restricted isometry property (RIP) condition,[15] we can recover $\mathbf{x}$ by solving the following optimization problem:

$$\hat{\mathbf{x}} = \min_{\mathbf{x}}\{\|\mathbf{y} - \boldsymbol{\Phi}\mathbf{x}\|_2^2 + \zeta\|\mathbf{x}\|_1\}, \tag{7}$$

where ζ is the regularization parameter. After the afore-mentioned recovery, $\hat{\mathbf{x}}$ should be reshaped back into a matrix.

3 Azimuth-Range Decouple-Based L_1 Regularization Wide ScanSAR Imaging via ECS

In practical wide ScanSAR imaging, due to the recovered algorithm based on optimization problem in Eq. (7) needs to transfer the 2-D echo data into a vector and reconstruct the considered scene via 2-D matrix operation for every image point in turn, which leads to much more computational cost. Therefore, an azimuth-range decoupling operation is essential in the L_1 regularization-based wide ScanSAR imaging so as to make large-scale sparse reconstruction of the considered scene possible.

In this section, using ECS as the example of the recovery algorithm, we will demonstrate the proposed azimuth-range decouple-based L_1 regularization wide ScanSAR imaging approach in detail. To illustrate the proposed method intuitively and clearly, we first define some operating matrices of ECS algorithm[9] as shown in Table 1.

3.1 *Imaging Model*

According to Eq. (1), 2-D ScanSAR imaging model without down-sampling can be represented as

$$\mathbf{Y} = \boldsymbol{\Xi}\mathbf{X}, \tag{8}$$

where $\mathbf{Y} \in \mathbb{C}^{N_\eta\times N_\tau}$ is the 2-D echo data of the bursts in one subswath, $\mathbf{X} \in \mathbb{C}^{N_P\times N_Q}$ is the backscattered coefficient of the considered scene in one subswath, and $\boldsymbol{\Xi}$ is the radar system observation matrix.

Let $\mathcal{R}(*)$ indicates the ECS imaging procedure of one subswath in wide ScanSAR, thus the surveillance region of one subswath $\mathbf{X}$ can be reconstructed by the ECS algorithm as

$$\mathbf{X} = \mathcal{R}(\mathbf{Y}), \tag{9}$$

with $\mathcal{R}(\cdot)$ being

$$\mathcal{R}(\mathbf{Y}) = \{\mathbf{F}_\eta^{-1}[\mathbf{F}_\eta(\mathbf{Y}) \circ \boldsymbol{\Psi}_1\mathbf{F}_\tau \circ \boldsymbol{\Psi}_2\mathbf{F}_\tau^{-1} \circ \boldsymbol{\Psi}_3 \circ \boldsymbol{\Psi}_4 \circ \boldsymbol{\Psi}_5]\} \circ \boldsymbol{\Psi}_6, \tag{10}$$

where the symbol $\circ$ denotes the Hadamard product.

The concept of azimuth-range decoupling derives from the formation of SAR echo data from the reflectivity image $\mathbf{X}$ of the surveillance region. The radar system observation matrix $\boldsymbol{\Xi}$ can be used to obtain the echo data by performing an azimuth convolution $\boldsymbol{\Xi}_a$ on the reflectivity image to generate the phase history, a range azimuth migration operator $\mathcal{M}$ to generate 2-D curves, and

Table 1 Definition of operators in the proposed method.

Operator	Meaning
$\mathbf{F}_\tau$	Range Fourier transform
$\mathbf{F}_\eta$	Azimuth Fourier transform
$\mathbf{F}_\tau^{-1}$	Range inverse Fourier transform
$\mathbf{F}_\eta^{-1}$	Azimuth inverse Fourier transform
$\mathbf{H}_\tau$	Range down-sampling matrix
$\mathbf{H}_\eta$	Azimuth down-sampling matrix
$\mathbf{\Psi}_1$	Chirp scaling
$\mathbf{\Psi}_2$	Range cell migration correction, range compression, and secondary range compression
$\mathbf{\Psi}_3$	Phase correction
$\mathbf{\Psi}_4$	Antenna pattern correction
$\mathbf{\Psi}_5$	Removal of hyperbolic azimuth phase and introduction of linear frequency modulation
$\mathbf{\Psi}_6$	Desampling and fractional shifts

a range convolution $\mathbf{\Xi}_r$. Therefore, according to the above idea of the azimuth-range decoupling operation, the imaging model in Eq. (8) can be rewritten as

$$\mathbf{Y} = \mathbf{\Xi}\mathbf{X} = \mathcal{M}(\mathbf{\Xi}_a\mathbf{X})\mathbf{\Xi}_r = \mathcal{P}(\mathbf{X}), \tag{11}$$

where $\mathcal{P}(\cdot)$ is the echo simulation operator, the inverse procedure of the high-precision MF imaging, e.g., ECS algorithm $\mathcal{R}(*)$ in this paper, which can be presented as

$$\mathcal{P}(\mathbf{X}) = \mathbf{F}_\eta^{\mathrm{H}}\{[\mathbf{F}_\eta(\mathbf{X} \circ \mathbf{\Psi}_6^{\mathrm{H}})] \circ \mathbf{\Psi}_5^{\mathrm{H}} \circ \mathbf{\Psi}_4^{\mathrm{H}} \circ \mathbf{\Psi}_3^{\mathrm{H}}\mathbf{F}_\tau \circ \mathbf{\Psi}_2\mathbf{F}_\tau^{\mathrm{H}} \circ \mathbf{\Psi}_1^{\mathrm{H}}\}, \tag{12}$$

where $(\cdot)^{\mathrm{H}}$ is the conjugate transpose operator.

After performing random down-sampling of the echo data, Eq. (12) can be expressed as

$$\mathbf{Y}_{\mathrm{d}} = \mathbf{H}_\eta\mathbf{Y}\mathbf{H}_\tau = \mathbf{H}_\eta\mathcal{P}(\mathbf{X})\mathbf{H}_\tau + \mathbf{N}_0, \tag{13}$$

where $\mathbf{Y}_{\mathrm{d}}$ is the 2-D downsampled echo data, $\mathbf{H}_\eta$ and $\mathbf{H}_\tau$ are the azimuth and range down-sampling matrices denoting the sparse sampling strategy, and $\mathbf{N}_0$ is a noise matrix.

Similar to the one-dimensional (1-D) wide ScanSAR reconstruction model in Eq. (7), for the 2-D model in Eq. (12), we can reconstruct the considered scene by

$$\hat{\mathbf{X}} = \min_{\mathbf{X}}\left\{\left\|\mathbf{Y} - \mathbf{H}_\eta\mathcal{P}(\mathbf{X})\mathbf{H}_\tau\right\|_{\mathrm{F}}^2 + \alpha\left\|\mathbf{X}\right\|_1\right\}, \tag{14}$$

where $\hat{\mathbf{X}}$ is the recovered 2-D image of the focused subswath, $\|\cdot\|_{\mathrm{F}}$ is the Frobenius norm of a matrix, and α is the regularization parameter.

3.2 *Iterative Recovery*

In our proposed method, ITA is used to solve the optimization problem [Eq. (14)]. The approximated sequence of solution is

$$\mathbf{X}^{(i+1)} = F\{\mathbf{X}^{(i)} + \mu^{(i)}[\mathcal{R}(\mathbf{H}_\eta^{\mathrm{T}}\{\mathbf{Y} - \mathbf{H}_\eta\mathcal{P}[\mathbf{X}^{(i)}]\mathbf{H}_\tau\}\mathbf{H}_\tau^{\mathrm{T}})], \mu^{(i)}\alpha^{(i)}\}, \tag{15}$$

where $(\cdot)^{\mathrm{T}}$ is the transpose operator, $F(\cdot)$ is the thresholding operator.[14] In Eq. (15), there are two critical parameters, μ and α, that control the iterative procedure, which are set adaptively to the iteration step as shown in Table 2. Normalized parameter μ controls the convergence speed of the iterative algorithm, whereas regularization parameter α controls the reconstructed precision.

Let $\mathbf{Z}^{(i)} = \mathbf{X}^{(i)} + \mu^{(i)}[\mathcal{R}(\mathbf{H}_\eta^{\mathrm{T}}\{\mathbf{Y} - \mathbf{H}_\eta\mathcal{P}[\mathbf{X}^{(i)}]\mathbf{H}_\tau\}\mathbf{H}_\tau^{\mathrm{T}})] \in \mathbb{C}^{N_P \times N_Q}$. The thresholding operator $F[\mathbf{Z}^{(i)}, \mu^{(i)}\alpha^{(i)}]$ is defined in terms of components as

$$F[\mathbf{Z}^{(i)},\mu^{(i)}\alpha^{(i)}] = \begin{Bmatrix} f[\mathbf{Z}^{(i)}(1,1),\mu^{(i)}\alpha^{(i)}] & f[\mathbf{Z}^{(i)}(1,2),\mu^{(i)}\alpha^{(i)}] & \cdots & f[\mathbf{Z}^{(i)}(1,N_Q),\mu^{(i)}\alpha^{(i)}] \\ f[\mathbf{Z}^{(i)}(2,1),\mu^{(i)}\alpha^{(i)}] & f[\mathbf{Z}^{(i)}(2,2),\mu^{(i)}\alpha^{(i)}] & \cdots & f[\mathbf{Z}^{(i)}(2,N_Q),\mu^{(i)}\alpha^{(i)}] \\ \vdots & \vdots & \ddots & \vdots \\ f[\mathbf{Z}^{(i)}(N_P,1),\mu^{(i)}\alpha^{(i)}] & f[\mathbf{Z}^{(i)}(N_P,2),\mu^{(i)}\alpha^{(i)}] & \cdots & f[\mathbf{Z}^{(i)}(N_P,N_Q),\mu^{(i)}\alpha^{(i)}] \end{Bmatrix}. \tag{16}$$

For the element $f(\mathbf{Z}^{(i)}(n_P, n_Q), \mu^{(i)}\alpha^{(i)})$ with $n_P = 1,2,\ldots,N_P$ and $n_Q = 1,2,\ldots,N_Q$ in Eq. (14), the iterative operation can be expressed as

$$f[\mathbf{Z}^{(i)}(n_P,n_Q),\mu^{(i)}\alpha^{(i)}] = \begin{cases} \mathrm{sgn}[\mathbf{Z}^{(i)}(n_P,n_Q)][|\mathbf{Z}^{(i)}(n_P,n_Q)| - \mu^{(i)}\alpha^{(i)}], & \text{if } |\mathbf{Z}^{(i)}(n_P,n_Q)| > \mu^{(i)}\alpha^{(i)} \\ 0, & \text{otherwise.} \end{cases} \tag{17}$$

The detailed procedure of ITA is shown in Table 2, where the absolute value operator is applied to a matrix elementwise. $\Delta\mathbf{X}_k^{(i)}$ equals to $\Delta\mathbf{X}^{(i)}$ at the support of $\mathbf{X}^{(i-1)}$ and equals to zero otherwise. $|\mathbf{X}^{(i)} + \mu\Delta\mathbf{X}^{(i)}|_{K+1}$ denotes the $(K+1)$ largest amplitude element of image $|\mathbf{X}^{(i)} + \mu\Delta\mathbf{X}^{(i)}|$ with K being a parameter representing the scene sparsity.

3.3 *Computational Cost*

In the following, we will discuss the computational complexity and the memory occupation of the proposed method in detail. For comparison, we also analyze the computational cost of conventional ECS and the L_1 regularization method. In the calculation, let I denote the required iterative steps; N_P and N_Q represent the pixels in the azimuth and range direction, respectively;

Table 2 ITA for azimuth-range decouple-based L_1 regularization wide ScanSAR imaging.

Input:	Echo data $\mathbf{Y}$
	Range and azimuth down-sampling matrix $\mathbf{H}_\tau$ and $\mathbf{H}_\eta$
Initial:	$\mathbf{X}^{(0)} = 0$
Iteration:	**While** $i \le I_{\max}$ and Residual $> \varepsilon$
Step 1:	$\mathbf{W}^{(i)} = \mathbf{Y} - \mathbf{H}_\eta\mathcal{P}[\mathbf{X}^{(i)}]\mathbf{H}_\tau$
Step 2:	$\Delta\mathbf{X}^{(i)} = \mathcal{R}[\mathbf{H}_\eta^{\mathrm{T}}\mathbf{W}^{(i)}\mathbf{H}_\tau^{\mathrm{T}}]$
Step 3:	$\mu^{(i)} = \|\mathbf{H}_\eta\mathcal{P}[\Delta\mathbf{X}_k^{(i)}]\mathbf{H}_\tau\|_F^2 / \|\Delta\mathbf{X}_k^{(i)}\|_F^2$
Step 4:	$\alpha^{(i)} = |\mathbf{X}^{(i)} + \mu^{(i)}\Delta\mathbf{X}^{(i)}|_{K+1}/\mu^{(i)}$
Step 5:	$\mathbf{X}^{(i+1)} = F[\mathbf{X}^{(i)} + \mu^{(i)}\Delta\mathbf{X}^{(i)}, \mu^{(i)}\alpha^{(i)}]$
Step 6:	Residual $= \|\mathbf{X}^{(i+1)} - \mathbf{X}^{(i)}\|_F$
Step 7:	$i = i + 1$
	End
Output:	Recovered image $\hat{\mathbf{X}} = \mathbf{X}^{(i)}$

$M_t = T_{\text{out}}/T_{\text{b}}$ represent the rate between the output azimuth extension T_{out} and the ScanSAR burst duration T_{b}, according to the discussion by Xu et al.[16] for ScanSAR imaging, the computational complexity of ECS is $C_{\text{ECS}} = \mathcal{O}[N_P N_Q M_t \log(N_P N_Q M_t)]$. For each iteration of our proposed method, its computation includes two main parts: the calculations of an inverse ECS and an ECS procedure, which have commonly the computational complexity of $\mathcal{O}[N_P N_Q M_t \log(N_P N_Q M_t)]$ and a decouple thresholding operation with complexity $\mathcal{O}(N_P N_Q M_t)$. Therefore, the total computational complexity of our proposed method is at the order $C_{\text{Pro}} = \mathcal{O}[I N_P N_Q M_t \log(N_P N_Q M_t)]$. While for the L_1 regularization method shown in Sec. 2, due to its need to transfer the 2-D echo data into a vector and reconstruct the considered scene via 2-D matrix operation for every image point in turn, the computational cost of it will reach $C_{L1} = \mathcal{O}(I N_P^2 N_Q^2)$, which is unacceptable for large-scale wide ScanSAR imaging. Compared with the conventional L_1 regularization approach, the accelerated rate of our proposed method is about

$$r_{\text{C}} = \frac{C_{L1}}{C_{\text{Pro}}} = \mathcal{O}\left[\frac{N_P N_Q}{M_t \log(N_P N_Q M_t)}\right]. \tag{18}$$

In memory occupation, since our proposed method needs only to store the input, output, and several matrices shown in Table 1, its memory occupation can be represented as $M_{\text{Pro}} = \mathcal{O}(N_P N_Q)$ bytes, which are at the same order as ECS algorithm. However, for conventional L_1 regularization method, due to it needs to transfer the 2-D echo data into a vector, construct the measurement matrix for every point of a considered scene in turn and perform the reconstruction based on the large measurement matrix, the memory need of it is very huge, about $M_{L1} = \mathcal{O}(N_P^2 N_Q^2)$ bytes.

From the above analysis, we can see that compared with the conventional L_1 regularization approach, the proposed method can reduce the computational complexity and memory occupation efficiently, which is at the same order as ECS-based SAR imaging algorithm.

4 Experiment and Discussion

In this section, we use TerraSAR-X wide ScanSAR focused data with six beams to illustrate the validity of our proposed imaging method. The data with 40-m azimuth resolution and 1.36-m slant range resolution were acquired at the west coast of Denmark on April 20, 2014 (see Fig. 2).

4.1 *Large-Scale Reconstruction*

Figure 3 shows the imaging results of one beam by means of conventional ECS and the proposed azimuth-range decouple-based L_1 regularization methods based on the full-sampling data. In Fig. 3, we can see that the proposed method not only can suppress clutter and sidelobe effectively for the oceanic area, a typical sparse scene, but also has achieved accurate recovery of the

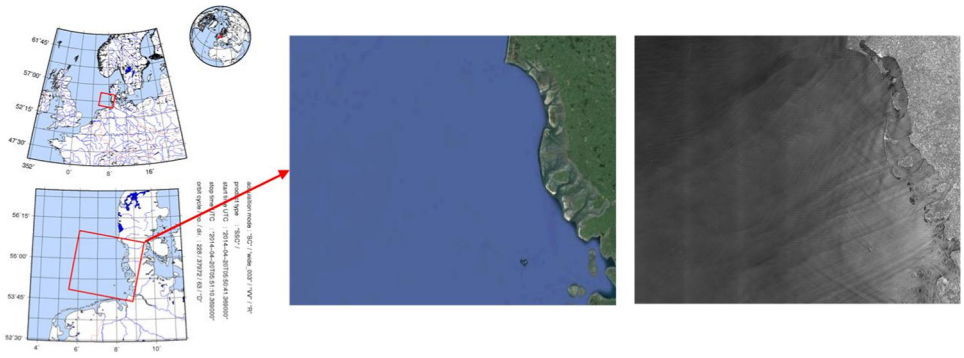

Fig. 2 Surveillance region of the TerraSAR-X wide ScanSAR data (optical image is from Google Earth).

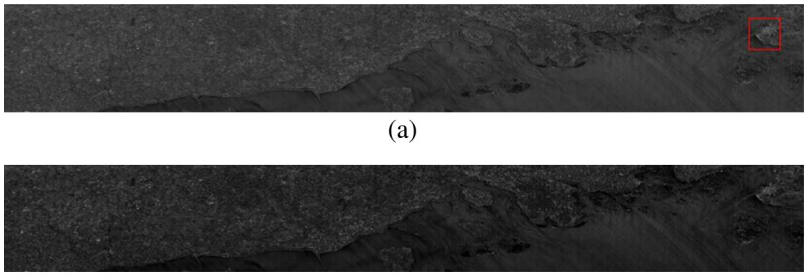

(a) (b)

Fig. 3 Reconstructed one beam of wide ScanSAR data via (a) ECS and (b) the proposed method.

nonsparse region (see Fig. 4). It is known that the conventional L_1 regularization SAR imaging technique only can be applied to the reconstruction of sparse scene because of the restriction of RIP condition and is not appropriate to the nonsparse region, e.g., urban area. However, our proposed method introduces an idea in the regularization reconstruction of the nonsparse surveillance region and makes large-scale regularization-based SAR imaging of the considered scene via full-sampling raw data possible, while it does not need to consider the sparsity of the surveillance region.

4.2 *Clutter Suppression*

Figures 5 and 6 are the reconstructed results by ECS and the proposed methods for ship- and wind-driven generators on the sea surface based on full-sampling data, respectively. We can see that compared with ECS, the proposed method can suppress the oceanic clutter and reduce sidelobes. To illustrate the effect of the proposed method in image performance improvement, we use the target-to-background ratio (TBR)[17] to evaluate the clutter suppression effect quantificationally which can be expressed as

$$\mathrm{TBR}(\mathbf{X}) \triangleq 20\log_{10}\left[\frac{\max_{(p,q)\in\mathcal{T}}\left|(\mathbf{X})_{(p,q)}\right|}{(1/N_{\mathcal{B}})\sum_{(u,v)\in\mathcal{B}}\left|(\mathbf{X})_{(p,q)}\right|}\right], \tag{19}$$

where (p,q) denotes the image pixel, and $\mathcal{T}$ is the target area that is surrounded by the background region $\mathcal{B}$, and $N_{\mathcal{B}}$ is the number of pixels in $\mathcal{B}$. We should note that the higher TBR is better.

The quantitative analysis of clutter suppression with TBR is depicted in Table 3. The results in Table 3 are in accord with the visual effect in Figs. 5 and 6, i.e., our proposed method outperforms the MF-based method when the clutter suppression effect is used for gauging the image performance.

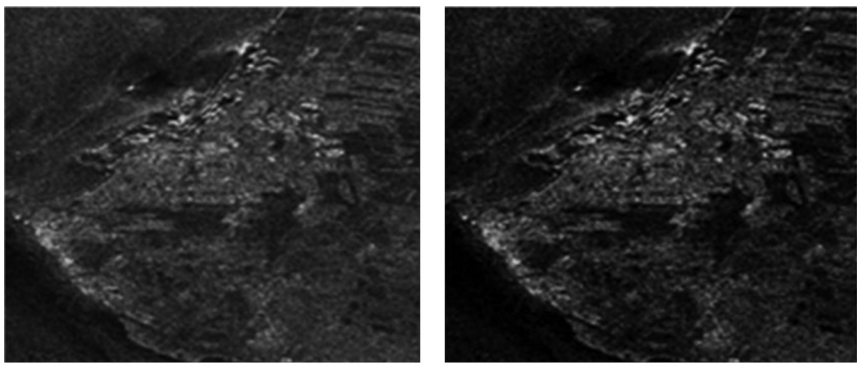

(a) (b)

Fig. 4 Reconstructed nonsparse surveillance region by (a) ECS and (b) the proposed method.

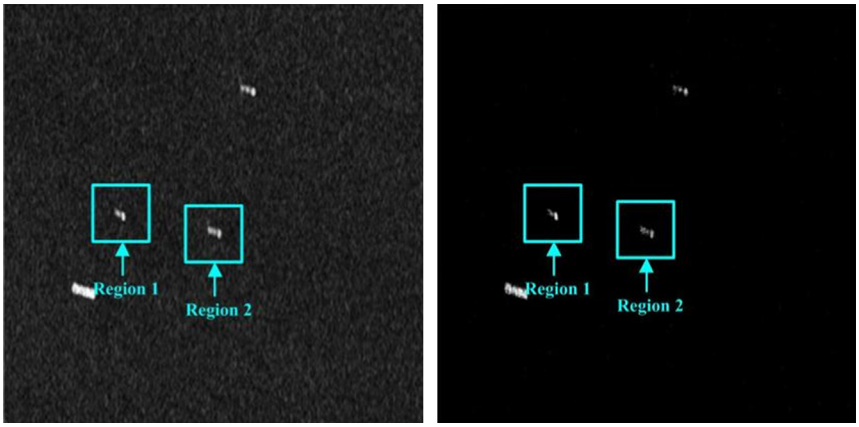

(a) (b)

Fig. 5 Reconstructed ships by (a) ECS and (b) the proposed method.

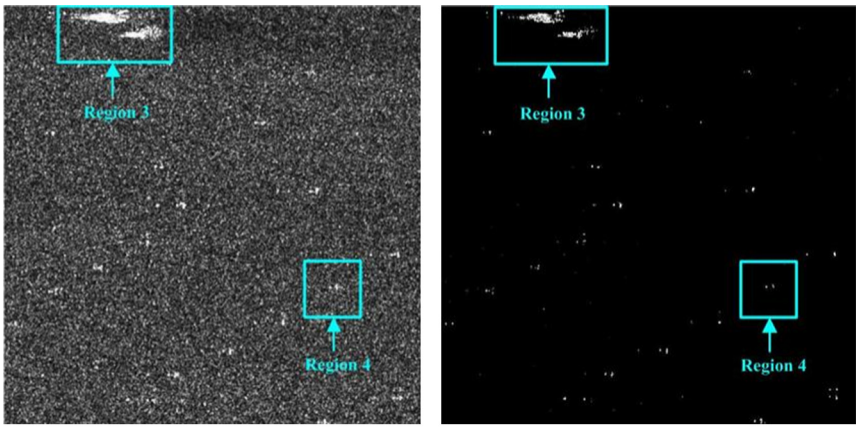

(a) (b)

Fig. 6 Reconstructed wind-driven generators by (a) ECS and (b) the proposed method.

Table 3 TBR of the selected regions in the images reconstructed by the ECS and the proposed method (dB).

Method	Region 1	Region 2	Region 3	Region 4
ECS	33.86	29.86	39.91	26.35
Proposed	60.31	53.96	59.66	51.59

4.3 *Super-Resolving*

Super-resolving is the potential of the L_1 regularization-based SAR imaging technique. Figure 7 shows the imaging results using ECS and the proposed methods based on full-sampling data. Compared with ECS, we find that the proposed method has higher resolution ability due to its suppressing clutter and sidelobes well (see the targets, especially in the red rectangles in Fig. 7). This means that our proposed method is suitable for the super-resolving imaging of the surveillance region.

4.4 *Downsampling Data-Based Regularization Reconstruction*

An advantage of the CS-based method is that it can recover the original sparse signals from far less samples than the well-known Shannon–Nyquist sampling theory requires. In this section, to

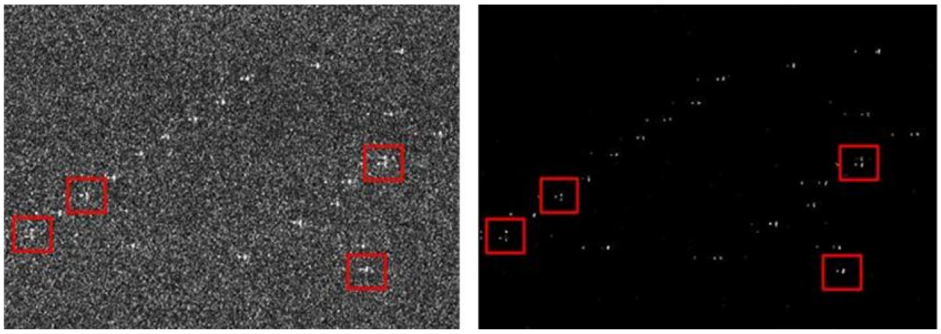

(a) (b)

Fig. 7 Imaging result via (a) ECS and (b) the proposed method.

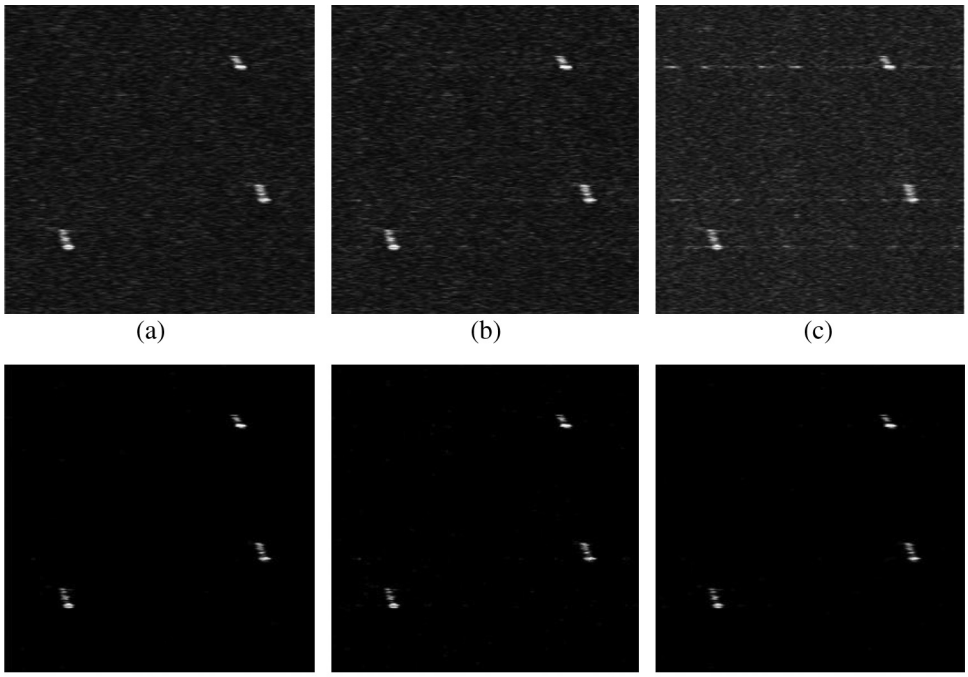

(a) (b) (c)

(d) (e) (f)

Fig. 8 Imaging result via ECS (upper row) and the proposed method (lower row) based on random down-sampling data. The sampling ratios are 100% (left column), 80% (middle column), and 50% (right column), respectively.

demonstrate the validity of the proposed method in ScanSAR imaging based on down-sampling data, we perform 80% and 50% random down-sampling for full-sampling echo data and reconstruct the surveillance region by ECS and the proposed method, respectively (see Fig. 8). Figure 8 shows that, due to the down-sampling, ECS could not recover the targets successfully with obvious ambiguities and energy dispersion. However, the proposed method also can reconstruct the considered scene successfully with lower sidelobes, noise, and clutter even only using 50% samples.

5 Conclusions

In this paper, we developed an ECS-based azimuth-range decouple L_1 regularization wide ScanSAR imaging method. On the one hand, for full-sampling ScanSAR raw data, the proposed method can improve SAR imaging performance efficiently compared with MF-based imaging

approaches (e.g., ECS in this paper), e.g., sidelobe, noise, and clutter suppression, for both sparse and nonsparse considered scenes and has potential in super-resolving imaging. On the other hand, it also can achieve high-resolution imaging for sparse scenes efficiently using down-sampling raw data. Compared with the conventional L_1 regularization imaging approach, our proposed method has less computational cost and hence makes large-scale regularization reconstruction of sparse considered areas possible. Experimental results via the real TerraSAR-X wide ScanSAR data verified our proposed method.

In addition, it should be noted that the proposed method is very helpful in practical ScanSAR system design. For large-scale sparse scene observation, e.g., ocean analysis, we can increase the swath width by decreasing PRF appropriately and use our proposed method to achieve high-resolution sparse reconstruction.

Acknowledgments

This work was supported by the Chinese Academy of Sciences/State Administration of Foreign Experts Affairs International Partnership Program for Creative Research Team and the National Natural Science Foundation of China under Grant No. 61571419.

References

1. J. C. Curlander and R. N. Mcdonough, *Synthetic Aperture Radar: System and Signal Processing*, Wiley, New York, NY (1991).
2. I. G. Cumming and F. H. Wong, *Digital Processing of Synthetic Aperture Radar Data: Algorithms and Implementation*, Artech House, Norwood, Massachusetts (2004).
3. R. K. Moore et al., "Scanning spaceborne synthetic aperture radar with integrated radiometer," *IEEE Trans. Aerosp. Electron. Syst.* **AES-17**(3) 410–421 (1981).
4. K. Thomas et al., "A global performance assessment approach for the TerraSAR-X staring spotlight and wide ScanSAR modes," in *10th European Conf. on Synthetic Aperture Radar (EUSAR)*, Berlin, Germany (2014).
5. H. Nyquist, "Certain topics in telegraph transmission theory," *Trans. Am. Inst. Electr. Eng.* **47**(2) 617–644 (1928).
6. C. E. Shannon, "Communication in the presence of noise," *Proc. Inst. Radio Eng.* **37**(1) 10–21 (1949).
7. A. M. Smith, "A new approach to range Doppler SAR processing," *Int. J. Remote Sens.* **12**(2) 235–251 (1991).
8. R. K. Raney et al., "Precision SAR processing using chirp scaling," *IEEE Trans. Geosci. Remote Sens.* **32**(4) 786–799 (1994).
9. A. Moreira, J. Mittermayerr, and R. Scheiber, "Extended chirp scaling algorithm for air- and spaceborne SAR data processing in stripmap and ScanSAR imaging modes," *IEEE Trans. Geosci. Remote Sens.* **34**(5) 1123–1136 (1996).
10. D. Donoho, "Compressed sensing," *IEEE Trans. Inf. Theory* **52**(4) 1289–1306 (2006).
11. E. Candès and T. Tao, "Near-optimal signal recovery from random projections: universal encoding strategies," *IEEE Trans. Inf. Theory* **52**(12) 5406–5425 (2006).
12. B. Zhang et al., "Sparse microwave imaging: principles and applications," *Sci. China Inf. Sci.* **55**(8) 1722–1754 (2012).
13. J. Fang et al., "Fast compressed sensing SAR imaging based on approximated observation," *IEEE J. Sel. Top. Appl. Earth Obs. Remote Sens.* **7**(1) 352–363 (2014).
14. I. Daubechies et al., "An iterative thresholding algorithm for linear inverse problems with a sparsity constraint," *Commun. Pure Appl. Math.* **57**, 1413–1457 (2004).
15. E. Candès, J. Romberg, and T. Tao, "Stable signal recovery from incomplete and inaccurate measurements," *Commun. Pure Appl. Math.* **59**(8) 1207–1223 (2006).
16. W. Xu, P. Huang, and Y. Deng, "A new imaging approach for burst mode synthetic aperture radar," *IEEE Trans. Aerosp. Electron. Syst.* **49**(3) 2035–2045 (2013).
17. M. Cetin et al., "Feature enhancement and ATR performance using nonquadratic optimization-based SAR imaging," *IEEE Trans. Aerosp. Electron. Syst.* **39**(4) 1375–1395 (2003).

Hui Bi received his bachelor's degree from YanTai University, Yantai, China, in 2012. Since September 2012, he has been working toward his PhD at the University of Chinese Academy of Sciences. Now he is also working in the Science and Technology on Microwave Imaging Laboratory, Institute of Electronics, Chinese Academy of Sciences, Beijing, China. His main research interests are sparse microwave imaging, synthetic aperture radar, and TomoSAR.

Bingchen Zhang received his bachelor's degree in electronic engineering and information science from the University of Science and Technology of China, 1996, and his master's degree from the Institute of Electronics, University of the Chinese Academy of Sciences, Beijing, in 1999. Since 1999, he has been working at the Institute of Electronics, Chinese Academy of Sciences as a scientist. His main research interests are sparse microwave imaging, synthetic aperture radar, radar signal processing, and radar systems.

XiaoXiang Zhu received her bachelor's degree in space engineering from the National University of Defense Technology, Changsha, China, in 2006. She received her master's degree, her doctor of engineering (Dr.-Ing.) degree, and her habilitation in the field of signal processing from the Technical University of Munich (TUM), Munich, Germany, in 2008, 2011, and 2013, respectively. Since 2011, she has been a scientist with the Remote Sensing Technology Institute at the German Aerospace Center (DLR), Oberpfaffenhofen. In 2015, she was appointed as a professor for signal processing in earth observation at TUM.

Wen Hong received her PhD from BeiHang University, China, in 1997. She was with the Department of Electrical Engineering, BeiHang University from 1997 to 2002. In between, she worked with the DLR-HF, Wessling, Germany, as a guest scientist from 1998 to 1999 for 1 year. Since 2002, she has been working at the Science and Technology on Microwave Imaging Laboratory as a scientist. Her main research interests are polarimetric/polarimetric interferometric SAR data processing and application, etc.